Vacancy trapping at tin atoms during the recovery of a fast-quenched dilute aluminium-tin alloy and its effect on the isomer shift of the ^{119}Sn Mossbauer isotope

1990 J. Phys.: Condens. Matter 2 3201

(http://iopscience.iop.org/0953-8984/2/14/005)

J. Phys.: Condens. Matter 2 (1990) 3201–3217. Printed in the UK

Vacancy trapping at tin atoms during the recovery of a fast-quenched dilute aluminium–tin alloy and its effect on the isomer shift of the ^{119}Sn Mössbauer isotope

Cs Szeles, K Süvegh, Z Homonnay and A Vértes
Laboratory of Nuclear Chemistry, Eötvös Loránd University, Budapest, H-1518 Hungary

Received 1 February 1989, in final form 23 November 1989

Abstract. Vacancy trapping at tin atoms during stage III and stage IV recovery as well as tin precipitation were studied in a fast-quenched Al–0.014 at.% Sn alloy by parallel positron lifetime and Mössbauer spectroscopy. The results show that the substitutional ^{119}Sn isotope with a trapped vacancy has 2.275 mm s^{-1} isomer shift. Trapping of more vacancies may cause significant line shift and leads to the appearance of a line at 2.86 mm s^{-1} in the Mössbauer spectra. The origin of this line position was interpreted as the relaxation of substitutional tin atoms to tetrahedral and octahedral interstitial positions in the centre of the vacancy clusters nucleated at the tin atoms. The defect recovery taking place in the alloy was found to be dominated by the strong tin–vacancy interaction. In stage III annealing, both vacancy annihilation and the formation of vacancy clusters independent of tin atoms are considerably suppressed by the strong trapping of vacancies at tin atoms. In stage IV recovery, the dissolution of dislocation loops, the migration of tin–multivacancy complexes and the formation of tin–atom clusters were observed. Precipitation of metallic tin exhibits several substages. The positron trapping observed upon precipitation was ascribed to the mismatch free volumes at the incoherent particle–matrix interface of the precipitates.

1. Introduction

Trapping of vacancies by impurities upon annealing of quenched and irradiated FCC metals has gained considerable interest in recent years due to the major developments in defect-sensitive microscopic methods such as pertubed angular correlation, ion channelling, diffuse x-ray and neutron scattering, field-ion microscopy, Mössbauer spectroscopy, positron annihilation, etc. These studies have mainly focused on the details of the early stage of vacancy trapping and clustering, the geometry of the small clusters and their growth mechanism, which are beyond the accessibility of the classical methods of electrical resistivity and transmission electron microscopy (TEM). All these methods have their own power and limitations concerning certain aspects of the aforementioned problems. The simultaneous application of two or more methods may therefore help to gain a considerably deeper understanding of the phenomenon studied. In the study reported here we have used both positron lifetime and Mössbauer spectroscopy to study the tin–vacancy interaction in fast-quenched aluminium and its effect on vacancy recovery, tin precipitation and the isomer shift of the ^{119}Sn Mössbauer isotope.

Tin is a unique impurity in aluminium in many respects. Owing to its much larger atomic volume and different crystal structure, it has a very low solubility [1]. It is well

0953-8984/90/143201 + 17 $03.50

known that tin atoms strongly trap migrating vacancies during stage III annealing, and the tin–vacancy clusters formed are stable up to around 420 K [2–5]. The extraordinarily strong binding of vacancies to tin atoms is characterised by a very high (0.4 eV) binding energy [3–5]. Substitutional tin atoms serve as nucleation centres for vacancy clusters in aluminium, and, if the cluster size and geometry allow, a strong relaxation of the substitutional tin atom occurs to the interstitial site at the centre of the cluster [6–8]. The strong preference of tin atoms for open-volume crystal defects manifests itself also during precipitation [9, 10], which was found to be a highly vacancy-assisted process. It was argued that trapped vacancies are responsible for the strain-free precipitate–matrix interface observed at spherical tin precipitates in aluminium [10].

Tin–vacancy interaction and tin precipitation in aluminium were also studied by Mössbauer spectroscopy. However, the interpretation of the lines appearing in the Mössbauer spectra of quenched and ion-implanted dilute Al–Sn alloys is often contradictory [11–16]. In quenched samples, besides the metallic (β) tin component at 2.54 mm s^{-1}, generally two more lines were found. One line, with an isomer shift value between 2.25 and 2.35 mm s^{-1}, is commonly assigned to dissolved tin, namely to tin atoms at substitutional sites with 12 aluminium neighbours [11–16]. The other line, appearing in the 2.70–3.00 mm s^{-1} range, was interpreted in various ways, i.e. as tin–atom clusters [11, 15], as tin–vacancy complexes [12], as tin atoms surrounded by more vacancies [13, 14] and as tin atoms at the early stage of nucleation [16].

The motivation for this study was basically twofold: first, to study vacancy trapping and clustering around tin atoms in stage III annealing, their subsequent recovery and their effect on precipitation; and secondly, to approach the long-standing and intriguing questions of the effect of vacancies on the isomer shift of the ^{119}Sn Mössbauer isotope in aluminium and the origin of the line with isomer shift at around 2.86 mm s^{-1}.

2. Experimental details

The Al–0.014 at.% Sn alloy was made from 99.999% aluminium and 99.99% tin enriched to 90% in ^{119}Sn isotope. Samples were solution annealed at 886 K for an hour in air prior to the fast quench in a vertical furnace. They were quenched into two different quenching baths, either methanol–dry ice mixture at 183 K or aqueous HCl solution at 203 K. To remove the ice of the quenching solution from the surfaces of the sample discs, they were washed in methanol at 183 K, dried with a cold cotton swab, and transferred to liquid nitrogen. As the quenching rate is much higher in the case of HCl solution, this sample set was used for the isochronal annealing studies in the 203–523 K temperature range. The samples were annealed for 15 min in a prepared annealing bath of aqueous ethylene glycol solution below room temperature and in a furnace above it. After each annealing step, the samples were quenched in liquid nitrogen and kept there between the measurements. To ensure parallel measurements, the same sample set was used for both the positron lifetime and the Mössbauer effect measurements.

The Mössbauer measurements were carried out with a constant-acceleration-type spectrometer in absorption geometry. The gamma source was $Ca^{119}SnO_3$ of 1.85×10^8 Bq activity; all the isomer shifts refer to this source. Mössbauer spectra were recorded at 88 K in a liquid-nitrogen-flow cryostat and the spectra were evaluated by least-squares fitting of simple Lorentzians.

The positron lifetime measurements were performed with a conventional fast–slow coincidence system based on NE111 plastic scintillators, XP1021 photomultipliers and

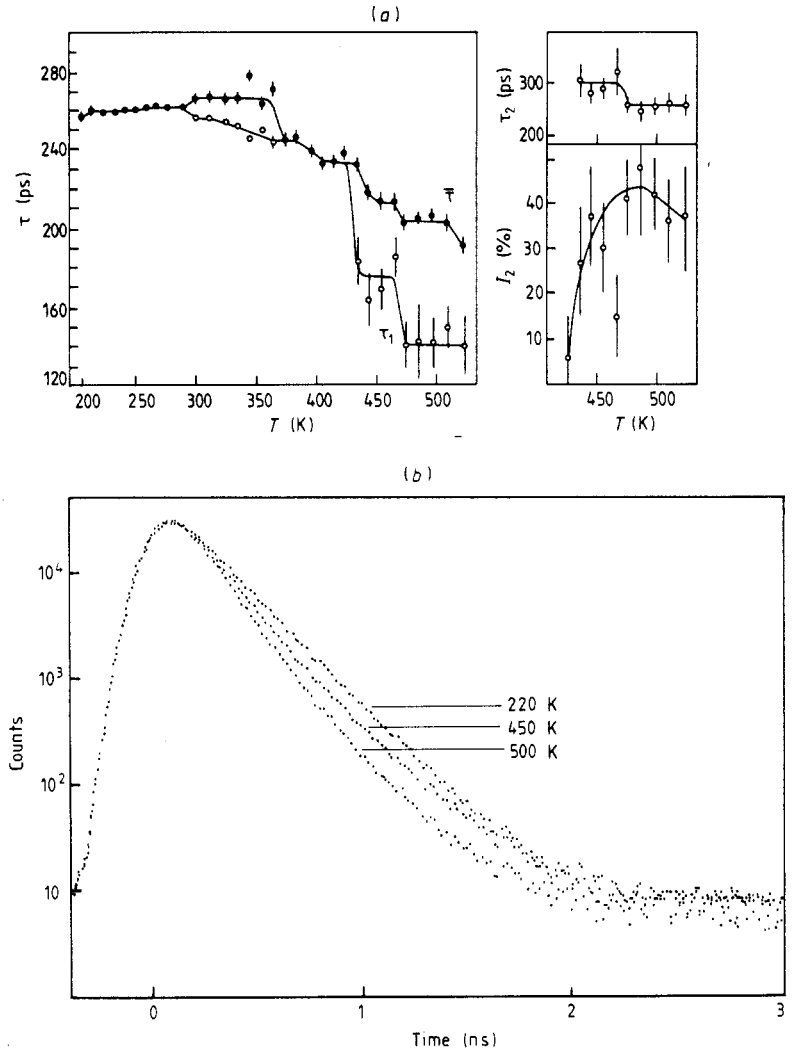

Figure 1. (*a*) Positron lifetime parameters ($\bar{\tau}$, τ_1, τ_2 and I_2) versus annealing temperature. (*b*) Typical positron lifetime spectra recorded at various annealing temperatures.

Ortec electronics. The time resolution of the system was 320 ps. The 3.7×10^6 Bq positron source was made by deposition of carrier-free ^{22}NaCl solution between 7.5 μm Kapton foils. To evaluate the spectra measured at 150 K, the RESOLUTION and POSITRONFIT programs were used [17].

3. Results

3.1. Isochronal annealing

The behaviour of the positron lifetime parameters versus isochronal annealing and typical lifetime spectra are shown in figures 1(*a*) and (*b*), respectively. Figure 2, on the

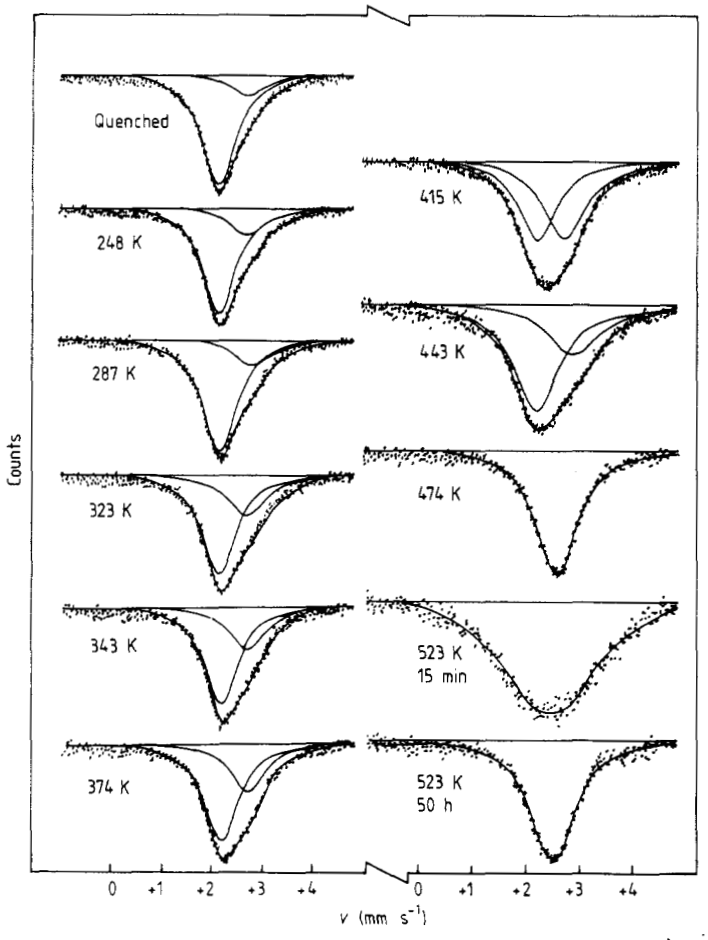

Figure 2. Mössbauer spectra recorded at various annealing stages. The full curves show the fitted Lorentzians.

other hand, shows the Mössbauer spectra at various annealing stages, while figure 3 displays the extracted parameters versus annealing temperature.

The lifetime spectra could be fitted well with a single 260 ± 2 ps component below 290 K. At 290–300 K, the mean lifetime ($\bar{\tau}$) increased to 266 ps and a poorly resolved, long component of 2–4% intensity appears in the spectra. Unfortunately the statistics of the spectra were too poor to extract reliable parameters for this long component. At 360–370 K, the long component disappears and the mean lifetime decreased to 245 ± 2 ps. Between 370 and 420 K, only the single-component fit of the spectra was found to be reliable. At 420–440 K, the sharp decrease of the mean lifetime from 233 ± 3 ps to 215 ± 3 ps is accompanied by the splitting of the spectra into two, well defined components.

The Mössbauer spectra could be evaluated with the assumption of two main lines below 443 K. One was observed with an almost constant isomer shift at 2.275 ± 0.005 mm s^{-1} (line 1), while the other appeared at 2.86 ± 0.1 mm s^{-1} (line 2). Only smaller changes were found in the parameters of these lines during the course of

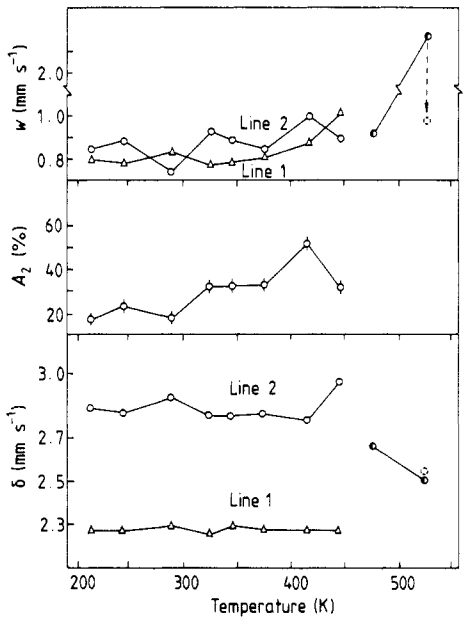

Figure 3. Isomer shifts (δ), linewidths (w) and relative area of line 2 (A_2) versus annealing temperature. Broken circles and the arrow show the change of the parameters upon 50 h annealing at 523 K.

isochronal annealing, except for the intensity of the second line, which exhibited striking annealing behaviour in steps corresponding rather well to the recovery observed in the positron lifetime parameters. Above 473 K, only one peak could be found in the spectra. Its isomer shift reached 2.57 mm s^{-1}, corresponding to β-tin, while its linewidth increased up to an extraordinarily high value of 2.16 mm s^{-1} after 523 K annealing. After a heat treatment for 50 h at 523 K, the linewidth decreased to 0.97 mm s^{-1}.

A separate line of less than 2% intensity was found at 0.00 mm s^{-1} in each Mössbauer spectrum due to SnO_2 formed on the surface of the sample during the 886 K solution annealing. (This was clarified by mechanically polishing test samples, which procedure removed this component from the spectra.) In order to reduce the number of fitting parameters in the evaluations, its isomer shift and linewidth at half-maximum were fixed to 0.00 and 0.80 mm s^{-1}, respectively [18, 19]. (This line is not shown in figures 2 and 3.)

It appears from the lifetime and Mössbauer data that the recovery of the fast-quenched Al–0.014 at.% Sn alloy took place in four distinct steps. These are summarised in table 1.

3.2. Methanol quench

In the samples quenched into methanol, only a single line was found with isometer shift of 2.28 mm s^{-1} and linewidth 0.85 mm s^{-1}, i.e. with the parameters of tin in solid solution. The positron lifetime spectra showed two components (table 2).

4. Discussion

4.1. Stage III annealing

It is well known from the 1960s [4, 20–22] that, in quenched and electron-irradiated pure aluminium, stage III recovery, namely the migration stage of vacancies resulting in the

Table 1. Recovery stages observed by positron lifetime and Mössbauer spectroscopy during isochronal annealing of the fast-quenched Al–Sn alloy.

Step	Positron lifetime		Mössbauer effect	
I	290–370 K	$\bar{\tau}$ increases: 260 → 266 ps. Low-intensity long component appears (290–300 K). $\bar{\tau}$ decreases: 266 → 245 ps. Long component disappears (360–370 K).	290–320 K	Two lines. A_2 increases: 21 → 30%
II	380–410 K	$\bar{\tau}$ decreases: 245 → 233 ps	370–415 K	A_2 increases: 30 → 50%
III	420–440 K	$\bar{\tau}$ decreases: 233 → 215 ps. Spectrum splits into two components. $\tau_2 = 300$ ps. I_2 increases: 10 → 40%	415–443 K	A_2 decreases: 50 → 30%. δ_2 shifts: 2.86 → 3.00 mm s^{-1}. Line broadening
IV	Above 470 K	τ_2 decreases: 300 → 255 ps	Above 470 K	Single line only. Line shift: 2.67 → 2.54 mm s^{-1}. Line broadening

Table 2. Results of the positron lifetime and Mössbauer effect measurements after fast quench into HCl and methanol and aging at room temperature following the methanol quench.

State of the samples	Positron lifetime				Mössbauer effect		
	τ_1 (ps)	τ_2 (ps)	I_2 (%)	$\bar{\tau}$ (ps)	δ_1 (mm s^{-1})	δ_2 (mm s^{-1})	A_2 (%)
HCl quenched	256 ± 2	—	—	256 ± 2	2.275 ± 0.005	2.86 ± 0.01	15 ± 2
Methanol quenched	206 ± 2	527 ± 23	7.2 ± 0.8	232 ± 2	2.280 ± 0.005	—	—
Aged at 295 K	201 ± 3	449 ± 47	4.2 ± 1.4	213 ± 2	2.280 ± 0.005	—	—

formation of vacancy clusters, occurs over the 200–300 K temperature range. The secondary defects formed at the beginning of this stage have been categorised according to their geometry or shape in the TEM photographs into three-dimensional clusters or voids and dislocation loops of various geometry. It was also observed that the addition to vacancies of small amounts of impurities with positive binding energy, like Mg, may considerably suppress the nucleation and growth of secondary defects due to the trapping of vacancies at these foreign atoms and their precipitates [23, 24]. In positron lifetime measurements the vacancy migration and condensation process appears as a dramatic decrease of the mean lifetime with the simultaneous appearance of a low-intensity long component with a lifetime in the 300–600 ps range [25, 26]. This behaviour is, however, distinctly different from that observed in the Al–0.014 at.% Sn alloy studied (figure 1), where the high and almost constant value of the mean positron lifetime (260 ± 2 ps) throughout stage III shows that no significant vacancy loss occurred below 290 K. The Mössbauer spectra also show remarkable stability characterised by a (21 ± 4)% intensity (A_2) of the second line.

4.1.1. The quenched state. The only resolved lifetime after the quench (256 ± 2 ps) and up till 290 K (260 ± 2 ps) is distinctly higher than the value characteristic of monovacancies generally found, in the 235–250 ps range experimentally [25–28] and 253 ps theoretically [29].

The absence of long-lifetime components and the very stable single-component lifetime spectrum with a 260 ± 2 ps lifetime suggests the following: first, that the positron trapping process is saturated (i.e. most of the positrons entering the samples are rapidly trapped in crystal defects and decay from localised states in these defects); secondly, that a significant fraction of the positrons decay from multivacancy defects; and thirdly, that the positron trapping is dominated by vacancy size defects.

Our attempts to resolve the lifetime spectra into two or more components in the 200–290 K temperature range failed, contraindicating any broad size distribution of defects, which would be a basic requirement to be able to decompose a separate lifetime component corresponding to the extended defects. In order to examine more closely the underlying distribution of the non-equilibrium vacancies responsible for the observed single-component lifetime spectra, we have performed an analysis on computer-generated multicomponent spectra. The spectra were generated using the relevant routines of the POSITRONFIT program [17] and appropriate statistical scatter [30]. We assumed that mono-, di-, tri-, tetra- and hexavacancies play the major role in the positron trapping process, and the lifetimes and intensities were calculated based on the well known simple multistate trapping model [27, 28], assuming various vacancy distributions. We applied the theoretical positron lifetimes [29] and the corresponding specific trapping rates [31] (from figure 9 of [31] for 150 K) to clusters of 1–6 vacancies in pure aluminium. The specific positron trapping rate to monovacancies was scanned between 2×10^{14} and $8 \times 10^{14}\,s^{-1}$, covering a good range of the experimental values published so far, $\mu_{1v} = (5.0 \pm 3.0) \times 10^{14}\,s^{-1}$ [32–34].

The results clearly show that a broad size distribution of defects, namely the presence of more extended open-volume defects in considerable concentration, is inconsistent with the single-component spectrum, and suggest that positron trapping is essentially dominated by monovacancies, divacancies (due to the high specific rate of the assumed resonance trapping to divacancies [31, 35]) and other defects with an apparent monovacancy positron lifetime. Moreover, the estimated vacancy concentration responsible for the high (260 ± 2 ps) mean lifetime is of the order of magnitude of or higher than the

total tin concentration of the samples (140 at. ppm), suggesting that a substantial fraction of the tin atoms (25–100%) have vacancy neighbours upon annealing in the 200–290 K annealing range.

The high initial lifetime shows that the vacancy loss rate during the quench is considerably lower in the alloy than in pure aluminium, resulting in a much higher vacancy supersaturation, and suggests the formation of vacancy clusters already during the quench. The interpretation of this effect is straightforward: the excess vacancies are those trapped at tin atoms during the course of the quench.

4.1.2. Vacancy annealing in stage III. The most important feature of the lifetime data recorded below 290 K is the stability of the single-component spectra with an essentially constant lifetime, 260 ± 2 ps. The trapping of mobile vacancies and small vacancy agglomerates at tin atoms and the saturated positron localisation already after the quench may easily explain the absence of any visible change in the positron lifetime spectra in the 200–290 K temperature range. Such a strong trapping of vacancies at tin atoms was found by ion-channelling experiments [6–8] at 220 K. This process produces a high number of tin–vacancy pairs and small tin–vacancy complexes, and may considerably suppress vacancy-cluster nucleation and growth at lattice sites independent of tin atoms. As strong relaxation of the tin atom towards the neighbouring monovacancy is probably negligible (see the discussion in section 4.1.3), the lifetime of the positron localised in the vacancy of the pair is very close to that in a vacancy without a tin neighbour. Hence the defect redistribution produced by vacancy trapping at tin atoms does not induce strong changes in the positron localisation characteristics and lifetime spectra, unless the vacancy clusters formed are large enough to enable relaxation of the tin atom.

Evidence on the suppression of dislocation-loop formation due to the trapping of vacancies at tin atoms in quenched Al–Sn crystals was provided by the TEM results of Kunstelj *et al* [10]. However, it is to be noted here that, although our interpretation also suggests strong vacancy trapping at tin atoms and infers significant suppression of vacancy clustering independently of tin atoms during stage III annealing, the formation of small voids and dislocation loops during the course of vacancy migration cannot be ruled out based on the positron lifetime data. Namely, it is well documented experimentally [28, 36, 37] that in pure aluminium the lifetime of positrons localised at dislocations and their loops is very close to the lifetime in monovacancies and, therefore, may give a contribution to the positron trapping that is practically indistinguishable from that of vacancies and tin–vacancy pairs. Hence it is very difficult to estimate the role of these defects in positron trapping; however, if present, they play an important role in the recovery process as both vacancy sinks and sources. Consequently, their presence cannot be excluded *a priori*, and we have to consider their possible effect on the recovery process too.

Little change was observed in the Mössbauer spectra below 290 K, indicating the stability of the corresponding tin-atom configurations. Contrary to this, at 290–300 K, the increase of the intensity of the second line and the appearance of a low-intensity long component in the lifetime spectra show intense defect redistribution. In this temperature range, the small vacancy clusters and voids are known to be unstable, and their dissolution and collapse take place in pure aluminium [25], so it is clear that the clusters formed in this stage and responsible for the long-lifetime component nucleate and grow at tin atoms.

The observed effect could be interpreted in two ways: either by the trapping of vacancies and small mobile vacancy associates, released during the dissolution of unstable vacancy clusters at or independent of tin atoms, at stable tin–multivacancy complexes, increasing their relative concentration; or by the transformation of unstable tin–multivacancy configurations to stable configurations. While the continuous decrease of the shorter-lifetime component from 255 ± 1 ps to 245 ± 3 ps supports the former, the disappearance of the long component from the lifetime spectra without any significant change in the Mössbauer spectra in the 360–370 K temperature range endorses the latter interpretation.

In conclusion, stage III recovery of the quenched dilute Al–Sn alloy observed by positron lifetime and Mössbauer spectroscopy could be plausibly interpreted by the trapping of mobile vacancies and small vacancy clusters at tin atoms below 290 K and by the transformation of unstable tin–multivacancy complexes to stable complexes in the 290–370 K temperature range.

4.1.3. The nature of the Mössbauer lines. The comparison of the Mössbauer and positron lifetime spectra of samples subject to HCl and methanol quenches (table 2) makes it very clear that the second Mössbauer line at 2.86 mm s^{-1} originates from tin atoms associated with vacancy complexes, as this line appears only in HCl quenched samples, where the retained vacancy concentration is much higher than in the methanol quenched samples due to the higher cooling rate in the former case. The simplest approach, namely that line 2 corresponds to tin–monovacancy pairs while line 1 corresponds to tin with perfect aluminium surroundings, could be ruled out immediately by considering the magnitude of positron trapping caused by these tin–vacancy pairs.

To get an estimate of the concentration of tin–vacancy pairs, we have to take into account the possible difference between the Lamb–Mössbauer factors of lines 1 and 2. Petersen and coworkers [13] found 165 ± 8 and 149 ± 11 K for the Debye temperatures and $f_1(300\ \mathrm{K})/f_2(300\ \mathrm{K}) = 1.3$ for the ratio of the Lamb–Mössbauer factors of lines with 2.27 and 2.99 mm s^{-1} isomer shifts, respectively, in their ion-implanted samples. Taking into account the precision of these values we get $f_1(88\ \mathrm{K})/f_2(88\ \mathrm{K}) = 1.1 \pm 0.1$ for our low-temperature data. Then from the value of the area of line 2 below 290 K, $A_2 = (21 \pm 4)\%$, one gets the concentration of tin atoms contributing to this line as 31 ± 7 at. ppm. A corresponding 31 ppm vacancy concentration, however, would result in a strongly split lifetime spectrum, with mean lifetime at most around 230 ps, rather than a single-component spectrum with 260 ± 2 ps lifetime. It is clear, therefore, that larger tin–vacancy clusters should be responsible for line 2.

Moreover, the high concentration of non-equilibrium vacancies retained in the HCl quench and the subsequent strong vacancy trapping at tin atoms during stage III annealing imply that a much higher fraction of tin atoms have vacancy neighbours than the ≈21% corresponding to line 2. This indicates that, besides line 2, the first line at 2.275 mm s^{-1} also corresponds to tin atoms with vacancy neighbours. The question is now to what configuration of tin–vacancy complexes these peaks actually correspond?

Three important features of the Mössbauer spectra should be emphasised here, which may serve as firm guidelines to address the question of the origin of the observed lines: first, the existence of only two lines in the spectra; secondly, the relatively small widths of these peaks, which never exceed 0.9 mm s^{-1} (below 290 K); and thirdly, the position of the second line (2.86 mm s^{-1}), which appears well outside the range defined by the isomer shifts of lines corresponding to tin dissolved in aluminium (2.28 mm s^{-1}) and in metallic (β) tin (2.57 mm s^{-1}).

The fact that we obtained no line broadening upon excessive vacancy trapping at tin atoms suggests that the vacancies sitting besides tin atoms have no significant effect on the isomer shift of the ^{119}Sn isotope, unless a subtle change occurs in the atomic configuration around the tin atom. The strong shift of the line position upon trapping of vacancies could then be plausibly associated with the relaxation of tin to the neighbouring vacancy cluster. The relaxation to interstitial positions causes a drastic change in the local symmetry of the atomic configuration, the effective atomic volume and the dynamic properties of the atom, which may be reflected by the s-electron density and isomer shift.

Evidence on tin relaxation towards the neighbouring vacancy clusters in aluminium was found by Swanson and coworkers [6–8] and Yagi and coworkers [38] in their He ion channelling and back-scattering studies. They observed relaxation of tin atoms to {1, 1, 1} planes (tetrahedral and octahedral interstitial positions) upon annealing at 220 K in irradiated [6–8] and Sn-implanted [38] samples. They proposed the interpretation that, by the trapping of vacancies migrating at 220 K [8] and produced during implantation [38], vacancy clusters are formed at tin atoms, and if their geometry is favourable the tin atoms relax towards the centre of the vacancy clusters, namely to the nearest interstitial positions. In this way tin–trivacancy, tin–tetravacancy and tin–hexavacancy clusters are formed (figures 4(*a*), (*b*) and (*e*)). This interpretation is in good agreement with the theoretical results. In particular, the self-interstitial–tetravacancy and self-interstitial–hexavacancy clusters were found to be among the energetically most favourable and hence most stable configurations of small vacancy agglomerates in FCC metals [39]. The solute–trivacancy cluster, on the other hand, was suggested to nucleate around ^{119}In atoms in nickel according to perturbed angular correlation studies [40]. In the case of tin atoms, which exhibit a large elastic misfit and hence a relatively large strain field in the aluminium matrix, relaxation to the vacancy cluster is expected to be even more favourable energetically as it may substantially decrease the strain energy, giving a large contribution to the driving force of solute–defect interaction [41].

Figure 4 shows the interstitial–tin–vacancy complexes suggested experimentally (figures 4(*a*), 4(*b*) and 4(*e*)) [8] and theoretically (figures 4(*c*) and (*d*)) [39]. It is very probable that in tin–monovacancy pairs substantial tin relaxation does not occur [8]. In this case the displacement of the tin atom towards the vacancy does not lead to energy gain but rather to energy increase, as the tin atom moves against the potential barrier set up by the four common nearest neighbours with the vacancy on the {1, 1, 0} plane. Only a slight relaxation is expected due to the small inward relaxation of the common nearest neighbours to the vacancy, which may partly decrease the elastic strain around the tin atom. The magnitude of this relaxation is, however, most probably much smaller than in the cases discussed above. Moreover, this implies that the characteristic positron lifetimes of vacancies and tin–vacancy pairs should hardly differ.

Unfortunately our understanding of the physics behind the isomer shifts of the ^{119}Sn Mössbauer isotope in metallic surroundings is far from satisfactory and theoretical efforts, particularly band-structure calculations are scarce [42, 43]. Attempts have been made to correlate the isomer shifts with the compressibilities of the host materials [44], the host atomic volumes [45] and the electronegativity of the matrix material [46]. Recently the semiempirical model of Miedema and van der Woude has been applied with some success to transitional metals [47, 48], but it failed in the case of ^{119}Sn isotope [49].

The isomer shift of tin in substitutional position in aluminium, 2.275 mm s^{-1}, is between the isomer shifts of α-tin, 2.00 mm s^{-1}, and β-tin 2.54 mm s^{-1} [18, 42, 43],

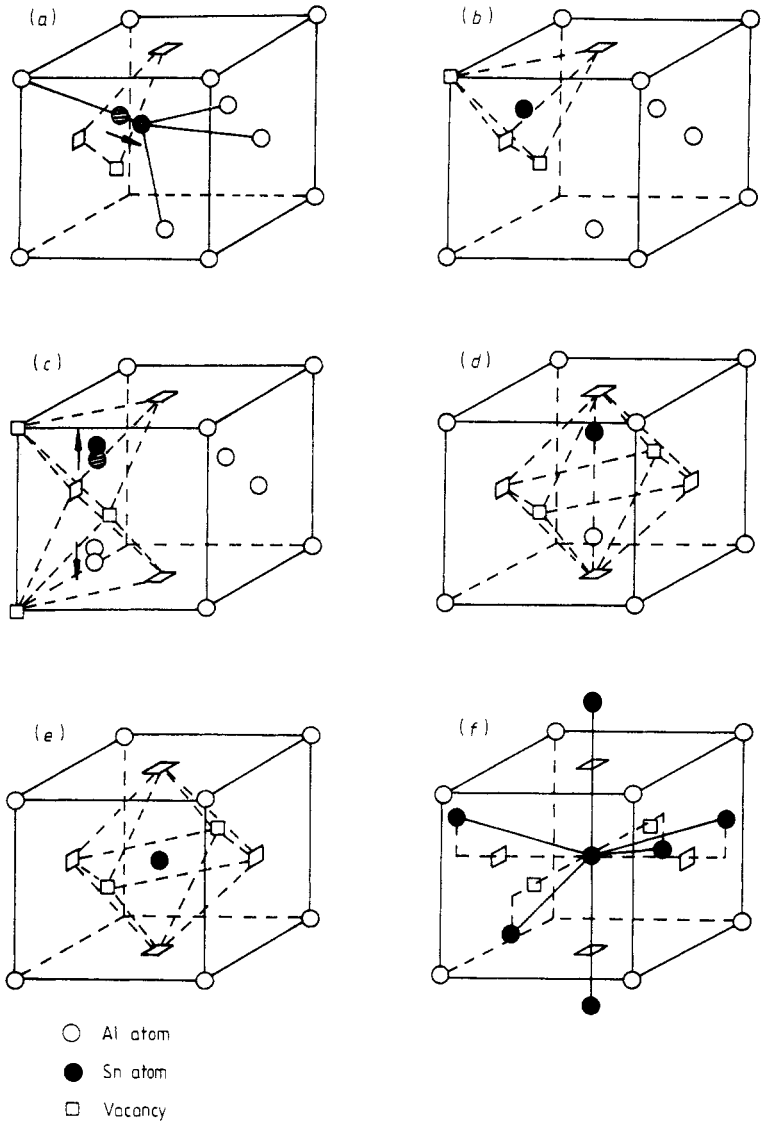

Figure 4. Relaxed interstitial-tin–vacancy clusters: (*a*) tin–trivacancy; (*b*) tin–tetravacancy; (*c*, *d*) di-interstitial–hexavacancy; (*e*) tin–hexavacancy; (*f*) an elementary tin-atom cluster at the octahedral tin–hexavacancy cluster. The cross-hatched circles and the arrows show the most probable relaxation of the atoms.

while that of interstitial-tin–vacancy clusters, 2.86 mm s^{-1}, is well outside this range. Considering the increasing packings of 34%, 53% and 74% of the diamond, body-centred tetragonal and FCC crystal structures of α-tin, β-tin and aluminium, respectively, as well as the increasing metallic character of the corresponding electron-band structure, the isomer shift of tin in aluminium appears very much out of order. A hint towards the understanding of both this surprising position and the isomer shift of tin atoms at tin–vacancy clusters could be deduced from the negative pressure dependence, and hence

Table 3. Nearest-neighbour distances relative to the aluminium lattice constant a and hard-sphere volumes in aluminium atomic volumes V_0 for the tin–vacancy clusters of figures 4(*a*)–(*e*).

	Number of vacancies	Number of nearest neighbours	Nearest-neighbour distance, d_{nn} (a)	Hard-sphere volume, V_{hs} (V_0)
4(*a*)	3	1, 4	0.58–0.65	0.34–0.81
4(*b*)	4	12	0.83	3.43
4(*c*)	6	1, 3, 12	0.50–0.83	0.09–3.43
4(*d*)	6	1, 5	0.72–0.75	1–1.96
4(*e*)	6	8	0.865	4.25
Al	—	12	0.72	1
Sn	—	4	0.76	1.81

positive volume dependence, of the isomer shift of β-tin [50, 51]. Recent electron band-structure calculations justified this negative pressure dependence and showed a decreasing occupancy of s-electron states with increasing pressure or decreasing atomic volume, resulting in the decrease of isomer shift upon compression [42]. It was suggested that the decrease of the occupancy of the s-electron states with pressure may be mediated by the contraction of the p-electron charge cloud [42, 50, 51].

The atomic volume of aluminium is about 30% less than the atomic volume of tin, and the nearest-neighbour distance in FCC aluminium is also 5% less than the nearest-neighbour distance in β-tin, accompanied by an increased coordination. Hence the tin atom in the aluminium matrix must be in a somewhat compressed state relative to β-tin even if a trapped monovacancy is present. The strong overlap with the aluminium valence electron shells may increase the hybridisation of the tin valence electrons (relative to the $5s^25p^2$ free-atom configuration) with a net decrease in the s-electron occupancy, in a way similar to that in β-tin upon decreasing the volume by compression, and may lead to the lower isomer shift value. This interpretation, moreover, gives a consistent explanation for the increase of the isomer shift when the effective free volume available for the tin atom increases upon relaxation of ^{119}Sn to the centre of the nearby vacancy cluster. In this case, similarly to the dilatation of the β-tin matrix, the valence electron configuration probably tends towards the atomic $5s^25p^2$ configuration, significantly increasing the contact density of s electrons at the nucleus, resulting in the increase of the isomer shift.

The effective volume available for the tin atoms may be very much different for the various clusters depending on the number of vacancies in the complexes and on the amount of relaxation of the tin and aluminium atoms. Very crude estimates using the hard-sphere model for the effective volume and the distance of tin atoms to the nearest-neighbour aluminium atoms are listed in table 3 for the complexes in figure 4, aluminium and β-tin. In the case of tin–trivacancy and di-interstitial–hexavacancy clusters, the data scan over a broad region depending on the degree of relaxation of the interstitial atoms. It appears from table 3 that the data of nearest-neighbour distances (d_{nn}) and hard-sphere volumes (V_{hs}) available for the tin atom practically fall into two groups. For the tin–trivacancy (4(*a*)) and octahedral di-interstitial–hexavacancy (4(*d*)) clusters, both

d_{nn} and V_{hs} are around or even less than that for tin at substitutional positions; consequently no big change is expected in the electron density upon tin relaxation. In the case of tin–tetravacancy (4(*b*)) and tin–hexavacancy (4(*e*)) clusters, on the contrary, both quantities increase significantly upon relaxation and they are both very close to each other. The separation of the data into two groups is particularly apparent for the nearest-neighbour distances, with a remarkably smaller scatter inside the groups. Considering the result that the ^{119}Sn isomer shift in FCC metals is, to a good approximation, proportional to the cube root of the valence electron density at the boundary of the Wigner–Seitz cell of the host metal [49], i.e. it scales with the interatomic distances rather than with the atomic volumes, it appears tempting from the data of table 3 to associate the observed two Mössbauer lines with these two groups of tin–multivacancy complexes.

The relaxation of tin atoms to the tin–trivacancy (4(*a*)) and octahedral di-interstitial (4(*d*)) configurations probably does not cause substantial isomer shift, as there is no significant increase in the nearest-neighbour distances and effective volume of the tin atom, suggesting that tin atoms in these configurations give a contribution to line 1. Line 2, with 2.86 mm s^{-1} isomer shift, on the other hand, may be associated with tin–tetravacancy (4(*b*)) and tin–hexavacancy (4(*e*)) clusters, as in this case intense increases in nearest-neighbour distance and atomic volume were observed. We have to emphasise, however, that the hard-sphere model employed here should be regarded only as a very crude and naive visualisation of the underlying physics. Electron band-structure calculations are necessary for a large variety of tin–vacancy clusters to establish a correlation between the configuration and size of the cluster around the tin atom and the Mössbauer isomer shift.

In conclusion, based on the structure of the Mössbauer spectra, on the line positions and widths, on the high vacancy concentration found by positron lifetime measurements and on the tin relaxation observed in ion-channelling experiments [6–8, 38], we propose that the Mössbauer line at 2.275 mm s^{-1}, besides substitutional tin with perfect surroundings, corresponds to tin–vacancy pairs and to those relaxed interstitial-tin–vacancy complexes or generally tin–defect complexes where the relaxation does not result in a substantial increase of the effective volume available for the tin atom. Hence tin atoms along dislocations, collapsed vacancy loops and larger dislocation loops may well give a contribution to this line. The line at 2.86 mm s^{-1} on the contrary we associate with relaxed interstitial-tin–vacancy clusters based on the tin–tetravacancy and tin–hexavacancy clusters.

4.2. Stage IV annealing

In contrast to pure aluminium where stage IV recovery occurs between 370 and 470 K in a single broad stage in the Al–Sn alloy, one finds that stage IV splits up into two distinct substages. In the first substage at 380–420 K the decrease of the only resolved lifetime from 245 ± 2 ps to 233 ± 3 ps and the increase of the intensity of the second Mössbauer line from 30% to around 50% was observed. In the second recovery substage at around 420–440 K the mean lifetime decrease to 215 ± 3 ps and the lifetime spectra split up into two components. The intensity of the longer component with 300 ± 25 ps lifetime increases to around 30%. Here the second line of the Mössbauer spectra slightly splits into a resonance doublet, it shifts to $\delta = 3.00$ mm s^{-1} and its intensity decreases to 30%.

4.2.1. The first substage. The first substage between 380 and 420 K practically coincides with stage IV annealing in pure aluminium [24, 52–54]. It is straightforward, therefore, to associate this substage with the dissolution, shrinkage and disappearance of dislocation loops, at or independent of tin atoms.

A change in the size of the dislocation loops is the result of the balance between the absorption and emission rate of vacancies at the loops. In stage IV recovery of aluminium, the shrinkage and dissolution of dislocation loops is known to be the result of a net loss of vacancies in a diffusion-controlled mechanism [53, 54], where vacancy concentration around the loops is in local equilibrium with the loops. The shrinkage rate of loops is therefore higher in the vicinity of vacancy sinks like dislocations, grain boundaries or precipitates of foreign atoms due to the trapping of the emitted vacancies, which decreases the vacancy concentration around the loops [52–54].

In our case the observed behaviour of the positron lifetime and Mössbauer spectra at around 380–420 K could well be interpreted by the shrinkage and dissolution of dislocation loops with the released vacancies trapped by tin atoms. The decrease of the mean positron lifetime shows the vacancy loss, while the increase of the intensity of the second Mössbauer line indicates the trapping of released vacancies at tin–vacancy complexes and an increasing fraction of tin atoms in tin–tetravacancy and tin–hexavacancy complexes due to the growth of smaller complexes.

4.2.2. The second substage. In the second substage between 420 and 440 K the splitting of the lifetime spectra into two components and the drastic decrease of the mean lifetime from 233 ± 3 ps to 215 ± 3 ps shows that the positron trapping is no longer saturated in traps with monovacancy lifetime, suggesting an excessive decrease of the number of small defects. The lifetime of the longer component (300 ± 25 ps) corresponds to di-, tri- and tetravacancies in pure aluminium [21] and this component may be associated with the relaxed tin–tetravacancy and tin–hexavacancy clusters. The increase of the intensity of this long component also reflects a significant decrease of the fraction of positrons decaying from smaller defects and an apparent increase of the fraction decaying from larger volume vacancy clusters.

The decrease of the intensity of the second Mössbauer line from 50% to 30%, on the other hand, shows an apparent decrease of the relative concentration of tin–multivacancy complexes.

This apparently contradictory behaviour of the positron lifetime and the Mössbauer spectra could be easily explained by the migration of tin–vacancy associates above 420 K [10, 16] and their agglomeration into complexes consisting of several tin atoms and vacancies. This process obviously decreases the concentration of both smaller and bigger tin–vacancy complexes. The resulting multi-tin–multivacancy complexes may well be responsible for the shift of the line position from 2.86 to 3.00 mm s^{-1} and the slight splitting of the second Mössbauer line into a doublet. The appearance of the resonance doublet in the spectra clearly shows the breakdown of the basic cubic symmetry around the tin atoms due to the formation of tin-atom pairs.

In conclusion, the two substages observed in stage IV recovery could be associated with the dissolution of dislocation loops and the migration of tin–multivacancy complexes, respectively. The tin-atom pairs and clusters formed in the later substage may serve as nucleation cores for β-tin precipitates.

4.3. Tin precipitation

At 473 K the two Mössbauer lines observed previously disappear and the spectrum could be fitted assuming a single line only with isomer shift of 2.68 mm s^{-1} and width

0.9 mm s^{-1}. This behaviour could be related to the diffusion and diminution of smaller tin–vacancy complexes and the growth of tin-atom clusters. The disappearance of the component at 2.275 mm s^{-1} shows that most of the isolated tin–vacancy pairs and tin–multivacancy complexes have merged into tin clusters or precipitates. This interpretation is supported by the lifetime results: the sharp decrease of the shorter lifetime value down to 140 ± 20 ps and a persistent increase of the long-component intensity (I_2) to 40% show strong condensation of the tin–vacancy pairs to vacancy clusters. The corresponding relatively low lifetime value $\tau_2 = 255 \pm 15$ ps above 470 K indicates that the size of the open-volume defects trapping positrons in this stage is around the size of mono- and divacancies. This decrease of the effective volume of the vacancy clusters around the tin atoms could be understood in terms of the higher interatomic distances in the β-tin crystal lattice.

It is to be noted here that the substitutional-tin–vacancy clusters may be considered as natural nucleation centres for tin atoms, as they allow easy accommodation of tin atoms in the semi-tetrahedral bonding configuration of the β-phase tin. This is illustrated in figure 4(f) where the elementary cluster of seven tin atoms, consisting of the semi-tetrahedral nearest-neighbour atoms plus the two next nearest neighbours residing slightly further away, was placed into the tin–hexavacancy complex. It is clear from the figure that the nearest-neighbour atoms easily take the distorted tetrahedral configuration by relaxing towards the six neighbouring octahedral positions.

The existence of open volumes at the incoherent boundaries of the tin precipitates is clearly shown by the high-intensity long component in the positron lifetime spectra exhibiting significant stability even at 523 K. This result is in very good agreement with the TEM observation that the tin precipitates formed in aluminium upon annealing at 473 K are spherical and do not show any strain-field contrast, indicating their strain-free accommodation in the matrix [10].

The isomer shift value of ^{119}Sn in the tin precipitates at 473 K ($\delta_2 = 2.68$ mm s^{-1}) is some 0.10 mm s^{-1} higher than the characteristic value for the β-phase particles, indicating a distorted crystal structure and/or high aluminium atom and vacancy content of the precipitates.

Upon annealing to 523 K the isomer shift nears 2.57 mm s^{-1}, namely the value characteristic for β-phase tin; however, the line broadens to a value 2.16 mm s^{-1}. Further annealing, for 50 h at 523 K, decreased the linewidth to 0.97 mm s^{-1} with apparently no change in the line position. The strong line broadening shows that the precipitation process occurring at a certain rate at 523 K sweeps through various stages. The unusual line broadening is most probably due to the appearance of quadrupole doublets with strong quadrupole splittings. However, the origin of this effect is unclear at the present stage of the investigation.

In conclusion, tin precipitation takes place in at least two steps: first, diffusion and condensation of the tin–multivacancy complexes; then, transformation of the formed tin-atom clusters was observed. Vacancies play a crucial role in both stages.

5. Conclusions

We have studied defect recovery during stage III and stage IV annealing as well as tin precipitation in a fast-quenched Al–0.014 at.% Sn alloy using positron lifetime and Mössbauer spectroscopy in parallel.

Based on the analysis of the positron lifetime spectra and the corresponding initial vacancy distribution after the quench, on the structure of the Mössbauer spectra, i.e. line positions and widths, and on the tin relaxation observed in ion-channelling experiments [6–8, 38], we assign both peaks appearing in the Mössbauer spectra to tin–vacancy associates. First, the resonance line at 2.275 mm s^{-1} was ascribed to tin atoms with perfect atomic surroundings, tin–vacancy pairs and to those tin–defect associates where the relaxation does not increase the effective free volume around the tin atom substantially. Secondly, the line at 2.86 mm s^{-1} was associated with relaxed interstitial-tin–multivacancy clusters based on the tin–tetravacancy and tin–hexavacancy complexes.

The interpretation of the four recovery steps observed in the isochronal annealing study (table 1) could be summarised as follows.

Stage III recovery of the alloy is dominated by the trapping of mobile single vacancies and small vacancy clusters at dissolved substitutional tin atoms. The formation of a large amount of tin–vacancy pairs results in a positron trapping dominated by monovacancies. The broad annealing stage, between 290 and 370 K, was interpreted by the transformation of unstable tin–multivacancy complexes to clusters stabilised by tin atoms (annealing step I).

Stage IV recovery of the alloy was observed to take place in two distinct substages. The stage at 380–420 K was associated with the dissolution of dislocation loops (annealing step II), while the stage above 420 K was associated with the migration of tin–multivacancy complexes (annealing step III).

The precipitation of tin occurring above 420 K was found to scan several stages. First, the diffusion and condensation of the tin–multivacancy complexes at 420–440 K (annealing step III), and then the transformation of the nucleated tin-atom clusters, above 470 K takes place (annealing step IV). The positron trapping observed upon precipitation was ascribed to the mismatch free volumes at the incoherent particle–matrix interface.

Acknowledgments

This work was supported by a grant from the Hungarian Science Foundation (OTKA). Cs Szeles wishes to express his thanks to the Faculty of Engineering of Tokyo University for hospitality during his contribution to the manuscript.

References

[1] Dorward R C 1976 *Metall. Trans.* **7A** 308
[2] Szeles Cs, Süvegh K, Homonnay Z and Vértes 1987 *Phys. Status Solidi* a **103** 397
[3] Kimura H and Hasiguti R R 1963 *J. Phys. Soc. Japan* **18** Suppl III, 73
[4] Federighi T 1965 *Lattice Defects in Quenched Metals* ed R M J Cotterill, M Doyama, J J Jackson and M Meshii (New York: Academic) p 217
[5] Fiorito G, Ceresara S and Federighi T 1966 *Acta Metall.* **14** 452
[6] Swanson M L and Maury F 1975 *Can. J. Phys.* **53** 1117
[7] Swanson M L, Howe L M and Quenneville A F 1980 *Phys. Rev.* B **22** 2213
[8] Swanson M L, Howe L M, Moore J A and Quenneville A F 1981 *J. Phys. F: Met. Phys.* **11** L185
[9] Erb U and Aust K T 1984 *Scr. Metall.* **18** 1263
[10] Kunstelj D, Pivac D, Rocak D, Stubicar M and Bonefacic A 1976 *Phil. Mag.* **34** 67
[11] Kato M, Ishida Y, Sassa K, Umeyama S and Mori M 1974 *J. Physique Coll.* **35** (C6) 309

[12] Umeyama S, Taniwaki M, Ishida Y and Kato M 1979 *J. Physique Coll.* **40** (C2) 539
[13] Petersen J W, Damgaard S and Weyer G 1981 *J. Phys. F: Met. Phys.* **11** 487
[14] Taniwaki M, Umeyama S and Ishida Y 1982 *Point Defects and Defect Interactions in Metals* ed J-I Takamura, M Doyama and M Kiritani (Tokyo: University of Tokyo Press) p 477
[15] Vértes A, Szeles Cs, Awad M Z, Nagy S and Lendvai A 1982 *Scr. Metall.* **16** 1229
[16] Szeles Cs, Süvegh K and Vértes A 1986 *Age-Hardenable Aluminum Alloys (Materials Science Forum 13/14)* ed I Kovács and J Lendvai (Aadermannsdorf: Trans. Tech.) p 511
[17] Kirkegaard P, Eldrup M, Mogensen O E and Pedersen N J 1981 *Comput. Phys. Commun.* **23** 307
[18] Flinn P A 1978 *Mössbauer Isomer Shifts* ed G K Shenoy and F E Wagner (Amsterdam: North-Holland) p 593
[19] Mehner H, Juhász J, Suba M and Vértes A 1982 *Radiochem. Radioanal. Lett.* **56** 57
[20] Doyama M and Koehler J S 1964 *Phys. Rev.* **134** A522
[21] Panseri C and Federighi T 1958 *Phil. Mag.* **3** 1223
[22] Schilling W, Burger G, Isebeck K and Wenzl H 1970 *Vacancies and Interstitials in Metals* ed A Seeger, D Schumacher, W Schilling and J Diehl (Amsterdam: North-Holland) p 255
[23] Smallman R E and Eikum A 1965 in [4], p 591
[24] Yoshida S, Kiritani M and Shimomura Y 1965 in [4], p 713
[25] Schaefer H E, Gugelmeier R, Schmolz M and Seeger A 1984 *Microstructural Characterization of Materials by Non Microscopical Techniques* ed H Andersen, M Eldrup, N Hansen, D Juul Jensen, T Leffers, H Lilholt, O B Pedersen and B N Singh (Roskilde: Risø National Laboratory) p 489
[26] Szeles Cs, Kajcsos Zs and Vértes A 1985 *Phys. Rev.* B **31** 1302
[27] Fluss M J, Smedskjaer L C, Chason M K, Legnini D G and Siegel R W 1978 *Phys. Rev.* B **17** 3444
[28] Aldi G, Dupasquier A, La Malfa U, Fiorentin S Re and Regazzoni C 1982 *J. Phys. F: Met. Phys.* **12** 389
[29] Puska M and Nieminen R M 1983 *J. Phys. F: Met. Phys.* **13** 333
[30] Sormann H, Kindl P and Puff W 1983 *Nucl. Instrum. Meth.* **206** 203
[31] Puska M and Manninen M 1987 *J. Phys. F: Met. Phys.* **17** 2235
[32] Fluss M J, Berko S, Chakraborty B, Lippel P and Siegel R W 1984 *J. Phys. F: Met. Phys.* **14** 2855
[33] Schaefer H E 1982 *Positron Annihilation* ed P G Coleman, S C Sharma and L M Diana (Amsterdam: North-Holland) p 369
[34] Jackman J A, Hood G M and Schultz R J 1987 *J. Phys. F: Met. Phys.* **17** 1817
[35] McMullen T and Stott M J 1986 *Phys. Rev.* B **34** 8985
[36] Linderoth S, Bentzon M D, Hansen H E and Petersen K 1985 *Positron Annihilation* ed P C Jain, R M Singru and K P Gopinathan (Singapore: World Scientific) p 494
[37] Smedskjaer L C, Manninen M and Fluss M J 1980 *J. Phys. F: Met. Phys.* **10** 2237
[38] Yagi E, Koyama A, Nakamura S, Sakairi H and Hashiguti R R 1985 *Japan. J. Appl. Phys.* **24** 137
[39] Crocker A G, Doneghan M and Ingle K W 1980 *Phil. Mag.* **41** 21
[40] Wichert Th, Deicher M, Echt O and Recknagel E 1978 *Phys. Rev. Lett.* **41** 1659
[41] Fiore N F and Bauer C L 1968 *Progress in Materials Science* vol 13, ed B Chalmers and W Hume-Rothery (Oxford: Pergamon) p 87
[42] Svane A and Antoncik E 1986 *Solid State Commun.* **58** 541
[43] Svane A and Antoncik E 1987 *Phys. Rev.* B **35** 4611
[44] Delyagin N N 1967 *Sov. Phys.–Solid State* **8** 2748
[45] Wagner F E and Wagner U 1978 in [18], p 433
[46] Watson R E and Benett L H 1978 *Phys. Rev.* B **17** 3714
[47] Miedema A R and van der Woude F 1980 *Physica* **100B** 145
[48] van der Woude F and Miedema A R 1980 *Solid State Commun.* **39** 1097
[49] Andreasen H, Damgaard S, Petersen J W and Weyer G 1983 *J. Phys. F: Met. Phys.* **13** 2077
[50] Moller H S and Mössbauer R L 1967 *Phys. Lett.* **24A** 416
[51] Moller H S 1968 *Z. Phys.* **212** 107
[52] Silcox J and Whelan M J 1960 *Phil. Mag.* **5** 1
[53] Siedman D N and Baluffi R W 1966 *Phil. Mag.* **13** 649
[54] Dobson P S, Goodhew P J and Smallman R E 1967 *Phil. Mag.* **16** 9